Real-space pseudopotential method for noncollinear magnetism within density functional theory

Doron Naveh, Leeor Kronik *

Department of Materials and Interfaces, Weizmann Institute of Science, Rehovoth 76100, Israel

ARTICLE INFO

ABSTRACT

We present a real-space pseudopotential method for first principles calculations of noncollinear magnetic phenomena within density functional theory. We demonstrate the validity of the method using the test cases of the Cr_3 cluster and the $Cr(\sqrt{3} \times \sqrt{3})R30°$ monolayer. The approach retains all the typical benefits of the real-space approach, notably massive parallelization. It can be employed with arbitrary boundary conditions and can be combined with the computation of pseudopotential-based spin-orbit coupling effects.

© 2008 Elsevier Ltd. All rights reserved.

Noncollinear magnetism, i.e., the absence of a spin quantization axis common to the whole system, is manifested in a wide variety of substances. Often, they arise as consequence of competing magnetic interactions in the same system (see, e.g., Refs. [1, 2] for an overview). One simple yet notable example is that of noncollinear magnetism arising from geometrically frustrated antiferromagnetic interaction. Such frustration is perhaps most easily visualized on two-dimensional triangular lattices (see, e.g., Refs. [3,4]), but can also be found in bulk structures [1,2] and has recently received much attention in the context of small transition metal clusters (e.g., refs. [5–16]).

There is obvious merit in describing noncollinear magnetic phenomena from first principles [2,17,18]. Specifically, it is interesting to employ density functional theory (DFT) [19], which has become the "work horse" of first principles calculations, towards studies of noncollinear magnetic phenomena. In principle, the generalization of the Hohenberg-Kohn theorem and the Kohn–Sham equation to spin-polarized systems, given by von Barth and Hedin [20], is not restricted to collinear magnetism. However, this aspect was not explored in practice until the work of Kübler et al. [21]. Early applications of this formalism all relied on the "atomic sphere approximation", where the spin-quantization axis at each point within a sphere around each atom was forced to be the same, but different spheres were allowed to

possess different axes [17,21]. Nordström and Singh have shown that this additional approximation is not necessary and have performed calculations where the magnetization density was a vector quantity that could vary continuously in direction as well as magnitude over all space [22].

The above ideas have been incorporated in different approaches to solving the Kohn–Sham equation. These include planewave-related methods, e.g., the linearized augmented planewave (LAPW) approach [22–24], the pseudopotential-planewaves approach [5, 25], and the projector augmented wave method, [6,26] as well as methods including both numerical [9,27] and gaussian [15] atomic basis sets.

A different effective method for solving the Kohn–Sham equation is to sample both wave functions and potentials on a real-space grid. In particular, the finite difference approach, where the kinetic energy is expressed as a high-order finite difference expansion [28], is a simple and powerful tool when used in conjunction with pseudopotentials. Among other advantages, it can be applied to non-periodic, partially periodic (e.g., surfaces), and fully periodic structures on equal footing, as it does not depend on a particular boundary condition [31]. In addition, it is readily amenable to massive parallelization, making it an attractive tool for studies of systems with a large number of atoms [30,32]. It is therefore desirable to account for noncollinear magnetism in real-space calculations, a task which we undertake here.

Insertion of the noncollinear spin density in the Kohn–Sham equations is made possible by a two-component spinor representation of the Kohn–Sham orbitals, $\phi_i(\vec{r})$. The Kohn–Sham equation

---

* Corresponding author.
  E-mail address: leeor.kronik@weizmann.ac.il (L. Kronik).

in terms of two components is [17]

$$\left(\left\{-\frac{1}{2}\nabla^2 + V_{ion}(\vec{r}) + V_H(\vec{r}) + V_{xc}[n,\vec{m}](\vec{r})\right\}\sigma_0 \right.$$
$$\left. + \vec{b}_{xc}[n,\vec{m}](\vec{r})\cdot\vec{\sigma}\right)\phi_i(\vec{r}) = \epsilon_i\phi_i(\vec{r}). \tag{1}$$

Here, $V_H(\vec{r})$ is the Hartree potential, $\vec{\sigma}$ is a vector of Pauli matrices, σ_0 is the 2×2 unit matrix, the charge and spin densities are given by

$$\vec{m}(\vec{r}) = \sum_{i=1}^{occ}\phi_i^\dagger(\vec{r})\vec{\sigma}\phi_i(\vec{r}) \tag{2}$$

$$n(\vec{r}) = \sum_{i=1}^{occ}\phi_i^\dagger(\vec{r})\phi_i(\vec{r}), \tag{3}$$

and the exchange correlation potential and magnetic exchange-correlation vector field are defined as

$$V_{xc}[n,\vec{m}](\vec{r}) = \frac{\delta E_{xc}[n,\vec{m}]}{\delta n}, \tag{4}$$

and

$$\vec{b}_{xc}[n,\vec{m}](\vec{r}) = \frac{\delta E_{xc}[n,\vec{m}]}{\delta\vec{m}}, \tag{5}$$

respectively. The general density in a noncollinear system has the form [7]

$$\tilde{n} = \frac{1}{2}(n\sigma_0 + \vec{m}\cdot\vec{\sigma}) = \frac{1}{2}\begin{pmatrix} n+m_z & m_x - im_y \\ m_x + im_y & n - m_z \end{pmatrix}, \tag{6}$$

where the explicit $\vec{r}$-dependence has been omitted for clarity. By diagonalizing this density at each point in space we obtain a local analogue of a collinear density

$$n_\pm = \frac{1}{2}(n \pm \|\vec{m}\|). \tag{7}$$

In the local spin density approximation (LSDA) [20], the spin density is parallel with the exchange-correlation magnetic vector field ($\vec{m} \parallel \vec{b}_{xc}$) [21]. The spin-dependent exchange-correlation potential and magnetic vector field can then be easily found from the functional derivatives in the locally collinear system:

$$\vec{b}_{xc} = \frac{1}{2}(V_{xc+} - V_{xc-})\hat{m}$$
$$V_{xc} = \frac{1}{2}(V_{xc+} + V_{xc-}). \tag{8}$$

This procedure is strictly valid only within the LSDA. It can also be employed with generalized gradient approximation (GGA) functionals that depend explicitly only on $n_\pm$ and $\nabla n_\pm$ [15], although it may be invalid for more general GGAs [29] and is not generally valid for an arbitrary functional form [24].

In the real-space approach to DFT, the wave-functions and potentials are sampled on a grid. The Hamiltonian matrix is neither calculated nor stored, but only operates on the trial wave-function in the process of diagonalization [30]. For evaluating the kinetic energy term, the Laplacian is expanded by finite differences. For an orthogonal grid, it is [28]

$$\nabla^2\psi_n = \sum_{m=-N}^{N}\frac{c_m}{h^2}[\psi_n(x_i + mh, y_j, z_k)$$
$$+ \psi_n(x_i, y_j + mh, z_k) + \psi_n(x_i, y_j, z_k + mh)], \tag{9}$$

where h is the grid spacing and c_n are the Nth order finite difference coefficients for the second derivative expansion.

In the pseudopotential approximation, core electrons are suppressed by replacing the true ionic potential with a pseudopotential that accounts for their effect. This facilitates grid-based calculations as it results in slowly varying potentials and wave functions. We employ nonlocal norm conserving pseudopotentials cast in the separable Kleinman–Bylander form [28,33]. In this form, the pseudopotential due to a single atom, $\hat{V}_{ion}^a$, is expressed as the sum of a local term and a nonlocal term, such that

$$\hat{V}_{ion}^a\psi_n(\vec{r}) = V_{loc}(|\vec{r}_a|)\psi_n(\vec{r}) + \sum_{l,m}G_{n,l,m}^a u_{l,m}(\vec{r}_a)\Delta V_l(|\vec{r}_a|), \tag{10}$$

where $\vec{r}_a = \vec{r} - \vec{R}_a$, $V_{loc}(|\vec{r}_a|)$ is the local component of the pseudopotential, $\Delta V_l(|\vec{r}_a|) = V_l(|\vec{r}_a|) - V_{loc}(|\vec{r}_a|)$, where $V_l(|\vec{r}_a|)$ is the pseudopotential corresponding to angular momentum l, $u_{l,m}(\vec{r}_a)$ is the pseudo-wave-function corresponding to angular momentum lm, and the projection coefficients are $G_{n,l,m}^a = \frac{1}{\langle\Delta V_{lm}^a\rangle}\int u_{lm}(\vec{r}_a)\Delta V_l(|\vec{r}_a|)\psi_n(\vec{r})d^3r$, where $\langle\Delta V_{l,m}^a\rangle = \int u_{lm}(\vec{r}_a)\Delta V_l(|\vec{r}_a|)u_{lm}(\vec{r}_a)d^3r$. The Kleinman–Bylander form is advantageous in real space because outside the pseudopotential core cutoff radius, r_c, $V_{loc}^a(\vec{r}_a) = -Z_{ps}/|\vec{r}_a|$, where Z_{ps} is the atomic number of the pseudoion, and $\Delta V_l(\vec{r}_a) = 0$. This limited nonlocality means that the real-space matrix is sparse.

Because of the exchange-correlation magnetic vector field, the dimensions of the Hamiltonian matrix must be doubled with respect to those used in a collinear spin calculation. Fortunately, the doubled Hamiltonian remains highly sparse because additional off-diagonal elements are introduced only on the diagonals of the off-diagonal blocks, namely:

$$\hat{H} = \begin{pmatrix} -\frac{1}{2}\nabla^2 + \hat{V}_{eff} + b_{xc_z} & b_{xc_x} - ib_{xc_y} \\ b_{xc_x} + ib_{xc_y} & -\frac{1}{2}\nabla^2 + \hat{V}_{eff} - b_{xc_z} \end{pmatrix}, \tag{11}$$

where $\hat{V}_{eff} = \hat{V}_{ion} + V_H + V_{xc}$. Note that for the collinear magnetic case $b_{xc_x} = b_{xc_y} = 0$, the elements on the off-diagonal blocks vanish, and one can diagonalize each diagonal block independently, as customary.

Importantly, the above Hamiltonian can be used with any type of boundary condition, be it non-periodic, fully periodic, or partially periodic [31]. Even if the lattice periodicity requires a non-Cartesian grid, the same formalism can be used with a generalized high-order finite-difference expression that avoids the numerical evaluation of mixed derivative terms [31].

The above concepts were implemented in the PARSEC software suite [30]. To test our approach, we chose to apply it to a Cr_3 cluster and to a free standing monolayer of chromium in a triangular lattice, both of which are known cases of noncollinear frustrated antiferromagnets [1–3,6,7,15,23,24,26]. We further chose to compare our results with those previously obtained with the Vienna ab initio software package (VASP) by Hobbs et al. [6, 26]. This is a stringent comparison because the description of non-collinear magnetism in VASP is different than in the present work. It is plane-wave-based and uses projector-augmented waves rather than pseudopotentials to describe the core electrons.

Our real-space pseudopotential calculations presented below were performed using the local spin density approximation (LSDA) for the exchange correlation functional [20]. Because chromium core states are not strongly bound, a multi-reference norm-conserving pseudopotential [34], as implemented in the atomic pseudopotentials engine (APE) software suite [35], was used. A reference configuration of $3s^23p^63d^54s^14p^0$ and cutoff radii (in a.u.) of $1.75/1.85/1.20/2.80/3.75$, respectively, were chosen, with the s component being the local one.

A map of the magnetic density vector, $\vec{m}$, of a Cr_3 cluster, in the cluster plane, is shown in Fig. 1. To facilitate comparison with

previous results [6], we chose an equilateral triangle with a bond length of 2.1 Å. The intensity of the color indicates the magnitude of the magnetization density and the arrows indicate its in-plane local direction. The magnetization density is characterized by intense "rings" around each atom, as it stems primarily from 3d–4s hybridized orbitals. The magnetization is close to collinear near each atom, supporting the usual picture of assigning a net direction for the magnetization of each atom, but there are significant regions of noncollinearity between the atoms. The total magnetic moment, integrated over all space, of the Cr_3 cluster is zero, as expected from symmetry. The magnetic moment per atom, however, calculated by integration of the magnetic moment within a sphere of 2 Å around each atom, is 2.86 Bohr magnetons (μ_B). All qualitative features of Fig. 1, as well as the quantitative value for the atomic magnetic moment, are in excellent agreement with previous work [6].

A map of the magnetic density vector, $\vec{m}$, of a free standing chromium layer in a $(\sqrt{3} \times \sqrt{3})R30°$ triangular lattice, in the layer plane, is shown in Fig. 2. The lattice parameter was fixed to fit the experimental lattice parameter of a hypothetical Ag(111) substrate, i.e., a bond length of 2.89 Å was used. Largely collinear magnetic domains at 120° to each other are observed, with boundaries that are more abrupt than in the Cr_3 cluster. The calculated magnetic moment per atom was 3.84 μ_B. Once again, these results are in excellent agreement with previous studies [23, 24,26] and the magnetic moment value is within 0.03 Bohr magnetons of the value reported by Hobbs et al., despite the use of LSDA here and GGA in Ref. [26].

Having proven the validity of our approach, we now turn to discussing its potential advantages. First, while we have used LSDA here for the sake of demonstration, the approach is, in principle, compatible with any functional, given a relation between n, $\vec{m}$ and V_{xc}, $\vec{b}_{xc}$. In particular, the pseudopotential real-space approach is well-suited for optimized effective potential (OEP) calculations within the exact exchange functional [36] and for orbital-dependent functionals in general [37]. This offers a natural means for noncollinear magnetism studies within the OEP approach, a combination which (to the best of our knowledge) has only been demonstrated once before [24]. Second, we have previously shown that addition of spin-orbit coupling via an appropriately constructed pseudopotential results in a Hamiltonian matrix which is similar in structure to that of Eq. (11). The only difference is that in the case of spin-orbit calculations entries in the off diagonal blocks are due to non-local pseudopotential projectors that contain an S_+ or an S_- term [38]. Clearly, the Hamiltonian entries due to spin-orbit coupling and due to the exchange-correlation magnetic vector field can be combined seamlessly. This would be important in, e.g., studies of magnetic anisotropy [39]. Last but not least, we expect that efficient massive parallelization [30,32] should be as easy to achieve as it is in standard real-space pseudopotential calculations.

In conclusion, we have presented a real-space pseudopotential method for first principles calculations of noncollinear magnetic phenomena within density functional theory. We demonstrated the validity of the method using the test cases of the Cr_3 cluster and the $Cr(\sqrt{3} \times \sqrt{3})R30°$ layer. The approach retains all the usual benefits of the real-space approach and is expected to be of benefit in future studies of noncollinear magnetic phenomena.

Acknowledgements

Fig. 1. Magnetic density map for a Cr_3 cluster, in the cluster plane. Color indicates the magnitude of the magnetic density and arrows indicate its local direction.
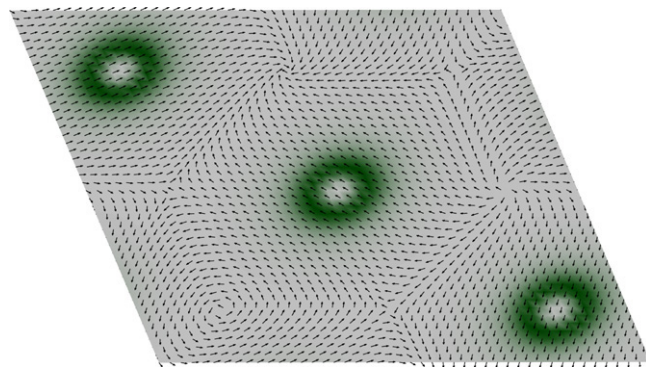
Fig. 2. Magnetic density map for a free standing $(\sqrt{3} \times \sqrt{3})R30°$ Cr monolayer, with periodic cell corresponding to the Ag(111) surface, in the layer plane. Color indicates the magnitude of the magnetic density and arrows indicate its local direction.

References

[1] J.M.D. Coey, Can. J. Phys. 65 (1987) 1210.
[2] L.M. Sandratskii, Adv. Phys. 47 (1998) 91.
[3] H. Kawamura, J. Phys.: Condens. Matter 10 (1998) 4707.
[4] D. Grohol, K. Matan, J.H. Cho, S.H. Lee, J.W. Lynn, D.G. Nocera, Y.S. Lee, Nature Mat. 4 (2005) 323.
[5] T. Oda, A. Pasquarello, R. Car, Phys. Rev. Lett. 80 (1998) 3622.
[6] D. Hobbs, G. Kresse, J. Hafner, Phys. Rev. B 62 (2000) 11556.
[7] C. Kohl, G.F. Bertsch, Phys. Rev. B 60 (1999) 4205.
[8] N. Fujima, Eur. Phys. J. D 16 (2001) 185; J. Phys. Soc. Japan 71 (2002) 1529.
[9] A.V. Postnikov, P. Entel, J.M. Soler, Eur. Phys. J. D 25 (2003) 261.
[10] R.C. Longo, E.G. Noya, L.J. Gallego, Phys. Rev. B 72 (2005) 174409.
[11] J. Mejía-López, A.H. Romero, M.E. Garcia, J.L. Morán-López, Phys. Rev. B 74 (2006) 140405(R).
[12] A. Bergman, L. Nordström, A.B. Klautau, S. Frota-Pessôa, O. Eriksson, Phys. Rev. B 75 (2007) 224245.
[13] M. Kabir, D.G. Kanhere, A. Mookerjee, Phys. Rev. B 75 (2007) 214433.
[14] L. Fernández-Seivane, Jaime Ferrer, Phys. Rev. Lett. 99 (2007) 183401.
[15] J.E. Peralta, G.E. Scuseria, M.J. Frisch, Phys. Rev. B 75 (2007) 125119.
[16] R.C. Longo, M.M.G. Alemany, J. Ferrer, A. Vega, L.J. Gallego, J. Chem. Phys. 128 (2008) 114315.
[17] W.E. Pickett, J. Kor. Phys. Soc. 29 (1996) S70.
[18] L.M. Sandratskii, P.G. Guletskii, J. Phys. F: Met. Phys. 16 (1986) L43.
[19] P. Hohenberg, W. Kohn, Phys. Rev. 136 (1964) B864;
W. Kohn, L.J. Sham, Phys. Rev. 140 (1965) A1133.
[20] U. von Barth, L. Hedin, J. Phys. C 5 (1972) 1629.
[21] J. Kübler, K.H. Höck, J. Sticht, J. Appl. Phys. 63 (1988) 3482;
J. Kübler, K.H. Höck, J. Sticht, A.R. Williams, J. Phys. F: Met. Phys. 18 (1988) 469.
[22] L. Nordström, D.J. Singh, Phys. Rev. Lett. 76 (1996) 4420.
[23] P. Kurz, F. Förster, L. Nordström, G. Bihlmayer, S. Blügel, Phys. Rev. B 69 (2004) 024415.
[24] S. Sharma, J.K. Dewhurst, C. Ambrosch-Draxl, S. Kurth, N. Helbig, S. Pittalis, S. Shallcross, L. Nordström, E.K.U. Gross, Phys. Rev. Lett. 98 (2007) 196405.
[25] G. Theurich, N.A. Hill, Phys. Rev. B 66 (66) (2002) 115208.
[26] D. Hobbs, J. Hafner, J. Phys.: Condens. Matter 12 (2000) 7025.

[27] V. García-Suárez, C. Newman, C. Lambert, J. Pruneda, J. Ferrer, Eur. Phys. J. B 40 (2004) 371377.

[28] J.R. Chelikowsky, N. Troullier, Y. Saad, Phys. Rev. Lett. 72 (1994) 1240;
J.R. Chelikowsky, N. Troullier, Y. Saad, Phys. Rev. B. 50 (1994) 11355.

[29] K. Capelle, G. Vignale, B.L. Györffy, Phys. Rev. Lett. 87 (2001) 206403.

[30] L. Kronik, A. Makmal, M.L. Tiago, M.M.G. Alemany, M. Jain, X. Huang, Y. Saad, J.R. Chelikowsky, Phys. Status Solidi (B) 243 (2006) 1063.

[31] A. Natan, A. Benjamini, D. Naveh, L. Kronik, M.L. Tiago, S.P. Beckman, J.R. Chelikowsky, Phys. Rev. B 78 (2008) 075109;
J. Han, M.L. Tiago, T.-L. Chan, J.R. Chelikowsky, J. Chem. Phys. 129 (2008) 144109;
M.M.G. Alemany, M. Jain, L. Kronik, J.R. Chelikowsky, Phys. Rev. B 69 (2004) 075101.

[32] J.R. Chelikowsky, A.T. Zayak, T.-L. Chan, M.L. Tiago, Y. Zhou, Y. Saad, J. Phys.: Condens. Matter (in press).

[33] L. Kleinman, D.M. Bylander, Phys. Rev. Lett. 48 (1982) 1425.

[34] C.L. Reis, J.M. Pacheco, J.L. Martins, Phys. Rev. B 68 (2003) 155111.

[35] M.J.T. Oliveira, F. Nogueira, Comput. Phys. Comm. 178 (2008) 524.

[36] S. Kümmel, L. Kronik, J.P. Perdew, Phys. Rev. Lett. 93 (2004) 213002.

[37] S. Kümmel, L. Kronik, Rev. Modern Phys. 80 (2008) 3.

[38] D. Naveh, L. Kronik, M.L. Tiago, J.R. Chelikowsky, Phys. Rev. B 76 (2007) 153407.

[39] See, e.g. O. Eriksson, J. Wills, in: H. Dreyssé (Ed.), Electronic Structure and Physical Properties of Solids: The Uses of the LMTO Method, Springer, Berlin, 2000, p. 247, and references therein.